Nonlinear aerostatic stability of a curved 275-m span suspension footbridge between Spain and Portugal

Miguel Cid Montoya

Texas A&M University – Corpus Christi, Corpus Christi, TX, USA

Juan Quintela, Santiago Hernández, José Ángel Jurado

Universidad de La Coruña, La Coruña, Galicia, España

Contact: miguel.cidmontoya@tamucc.edu

Abstract

This study reports the nonlinear aerostatic stability studies carried out for a suspension footbridge with a curved deck spanning 275 meters over the Miño River between Spain and Portugal. The footbridge's aerostatic performance is controlled by its highly aesthetic but complex three-dimensional configuration, the high slenderness of the deck, the construction process, and the aerodynamic characteristics of the triangular 4.5-meter-wide bluff deck cross-section, which demands a detailed aerodynamic study. The analysis is conducted using a nonlinear modal-based method recently developed by the authors. The deck's rotation is driven not only by the aerodynamic moment-induced rotation but also by the drag-induced rotation due to the configuration of the cable supporting system and, very significantly, by the lift-induced rotation due to the deck's curvature.

Keywords: footbridges; curved decks; suspension bridges; aerostatic stability; wind tunnel; dynamic analysis; root-finding algorithms; lift-induced rotation

1 Introduction

Curved footbridges are a very popular design alternative given their remarkable aesthetic attributes and its efficient structural performance. Notable examples are the Gateshead Millennium Bridge, Gateshead, UK, with 126 meters of main span, the Ponte de Mare, Pescara, Italy, which spans 172 m, and the Puente de Santa María de Benquerencia, Toledo, Castilla-La Mancha, Spain, 2011, spanning 170 m. However, the increasing span lengths adopted in contemporary projects turns wind-resistant analysis an important part of their design.

This study reports the nonlinear aerostatic stability studies carried out for a footbridge linking Goián-Tomiño (Pontevedra), Spain, with Vila Nova de Cerveira (Minho), Portugal. This suspension footbridge designed for pedestrians and cyclists spans 275 meters over the Miño River. Two pylons support the three-dimensional curved main cable of the suspension system that sustains the curved deck, as shown in the visualizations presented in Figure 1. The footbridge's aerostatic performance is

Figure 1. Visualization of the curved Goián footbridge over the Miño River (courtesy of Bernabeu Ingenieros).

controlled by its highly aesthetic but complex three-dimensional configuration, the high slenderness of the deck, the construction process, and the aerodynamic characteristics of the triangular 4.5-meter-wide bluff deck cross-section, which demands a detailed aerodynamic study. A 1:15 scale sectional model of the deck cross-section was built and tested at the aerodynamic wind tunnel (TUVA) of the University of La Coruña, Spain, to obtain the deck´s aerodynamic force coefficients as a function of the angle of attack. The nonlinear aerostatic stability analysis is carried out using a nonlinear modal-based method previously developed by the authors [1]. The analysis showed that the initial loads induced during the construction process impact the nonlinear structural responses. The deck's rotation is driven not only by the aerodynamic moment-induced rotation but also remarkably by the lift-induced rotation due to the deck's curvature, which is an interesting characteristic not commonly found in bridge aeroelasticity. The layout of the bridge and curvature of the deck are shown in Figure 2. These effects highlight the importance of performing nonlinear three-dimensional analysis to accurately assess the critical wind velocity. This study describes the stiffness degradation path from a modal perspective and discusses the impact of each nonlinear characteristic on the footbridge aerostatic stability analysis.

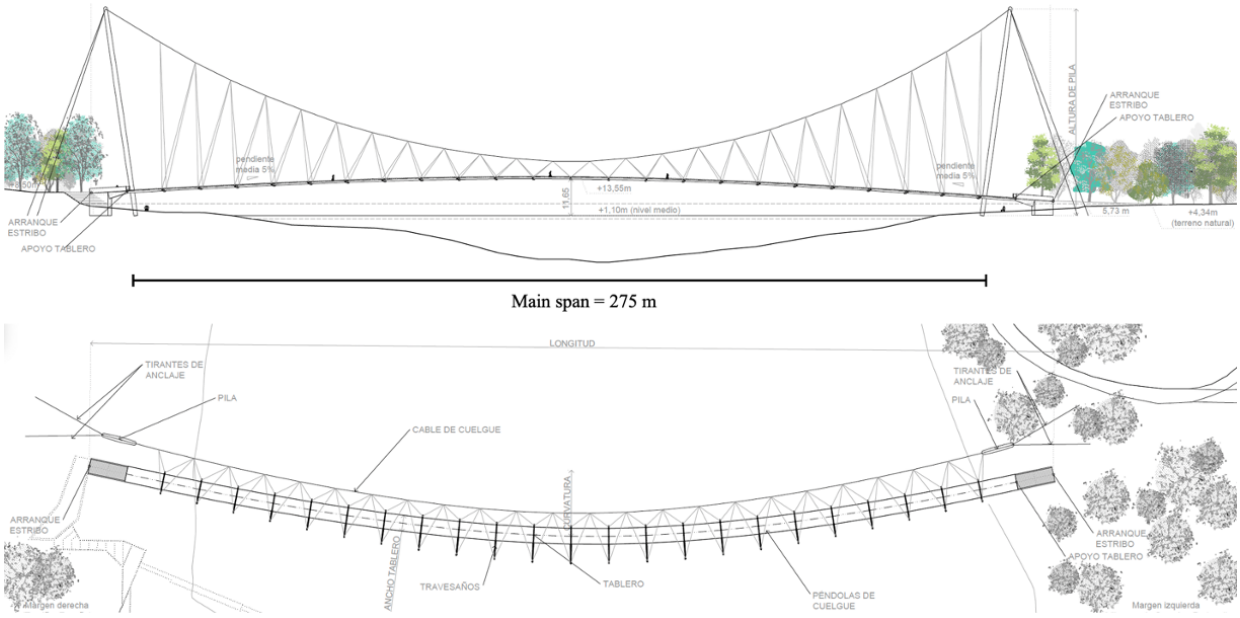

Figure 2. Layout of the Goián footbridge (courtesy of Bernabeu Ingenieros).

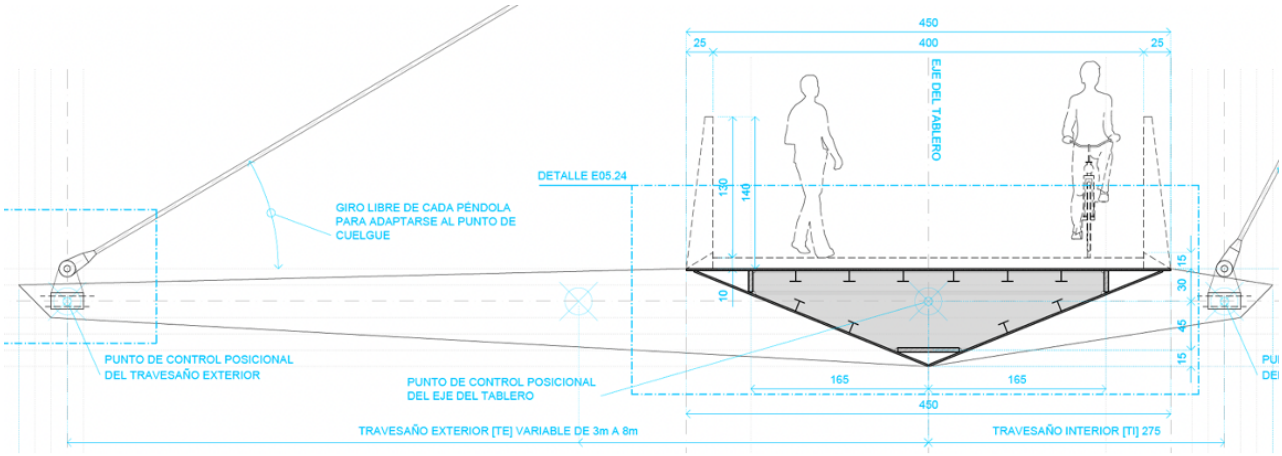

Figure 3. Detail of the deck cross-section and the asymmetric transversal beam (courtesy of Bernabeu Ingenieros).

2 The Goián footbridge: a long-span, slender, curved suspension footbridge

As part of the project Visit Rio Minho, there is a plan for the construction of a suspension footbridge linking the parks Espazo Fortaleza in Goián-Tomiño (Pontevedra), Spain, and O Castelinho in Vila Nova de Cerveira (Minho), Portugal. This footbridge designed for pedestrians and cyclists has a single span of 275 meters over the Miño River, allowing a clearance of 11.65 meters. Two 66.19-meter-tall pylons support the three-dimensional curved main cable of the suspension system. The deck cross-section adopted is a 4.5-meter-wide and 0.9-meter-deep triangular closed box. It is shown in Figure 3, where the transversal beams that permit the connections with the inclined hangers are shown. The following sections describe the construction process, the resulting initial deformation of the deck, and the dynamic properties of the deck in terms of mode shapes and natural frequencies. The low values of the natural frequencies and the bluff geometry adopted for the deck cross-section highlight the need for conducting a complete aeroelastic study, including wind tunnel tests and aeroelastic analyses in order to guarantee the desired performance of this slender long-span footbridge.

2.1 Construction process

The construction process of the pedestrian bridge consists of several phases that are summarized in Figure 4. Initially, the pylons of the footbridge are built with auxiliary temporary bracing, and lateral backstays are installed (Phase I). Once the pylons are in place, the main cable is installed (Phase II). Then, the deck is built by progressively adding segments in a sequential manner, starting from both ends of the deck and progressing toward the center of the span. Each deck section that is installed is secured by provisional stressed braces, and hangers are placed to connect it to the main cable (starting in Phase III of Figure 4). This process is carried out for all the segments of the deck. Finally, the central section of the deck is placed on provisional supports (Phase XI), and the corresponding hangers connecting it to the main cable are installed. Once the entire deck is in place, the provisional supports of the central section are removed (Phase XII), and the distressing and removal of the provisional braces for each deck section are carried out, removing them in reverse order of their placement, from the center of the deck towards the ends (Phases XII-XVI). Subsequently, the provisional bracing of the piers are removed, an initial stress of the main cable is applied, and the crawling of the deck takes place. Finally, a vertical overload is applied to the entire deck, and a final stress of the main cable is carried out (Phase XVIII).

All these construction stages were studied using a sequential lineal analysis in a 3D FEM built using SAP2000 and are calculated as initial steps before any wind calculation can be conducted since they allow the assessment of the actual deformation of the footbridge and accounts for all initial stresses.

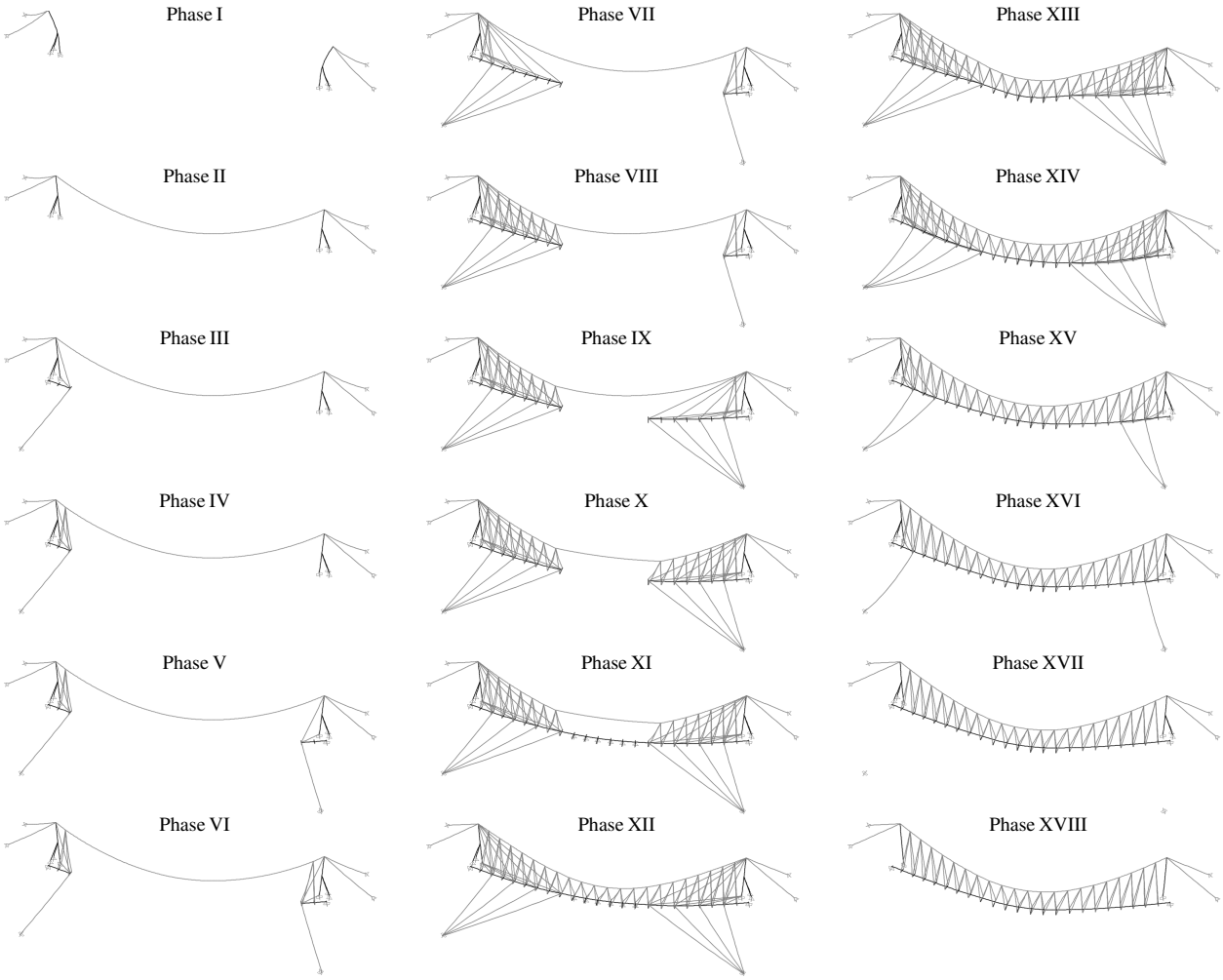

Figure 4. Construction stages of the footbridge that give place to the initial deformation of the footbridge layout. Visualization generated using SAP2000 and nonlinear static analyses.

2.2 Initial geometry

The initial geometry of the deck after the competition of the construction process is shown in Figure 5. This pattern and related initial stress levels will condition all displacements calculated during the nonlinear aerostatic analysis carried out to assess the aerostatic stability of the footbridge.

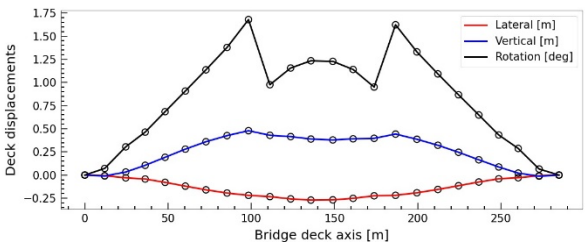

Figure 5. Initial deformation of the deck after the competition of the construction process.

2.3 Dynamic response

The footbridge dynamic response is required to use the aerostatic analysis method developed by the authors [1], which was previously and used in bridge, energy [2], and aerospace [3] applications. The dynamic properties of the footbridge are reported in Figure 6. The modes are normalized to the displacement and plotted along the bridge deck length. It is important to note that, due to the complex geometrical configuration of the footbridge and the curvature of the deck, most of the modes are a combination of lateral, vertical, and torsional components. This contrasts with the pure modes commonly obtained for bridges with straight layouts, where each mode usually shows displacements in one or two degrees of freedom, particularly in the first modes.

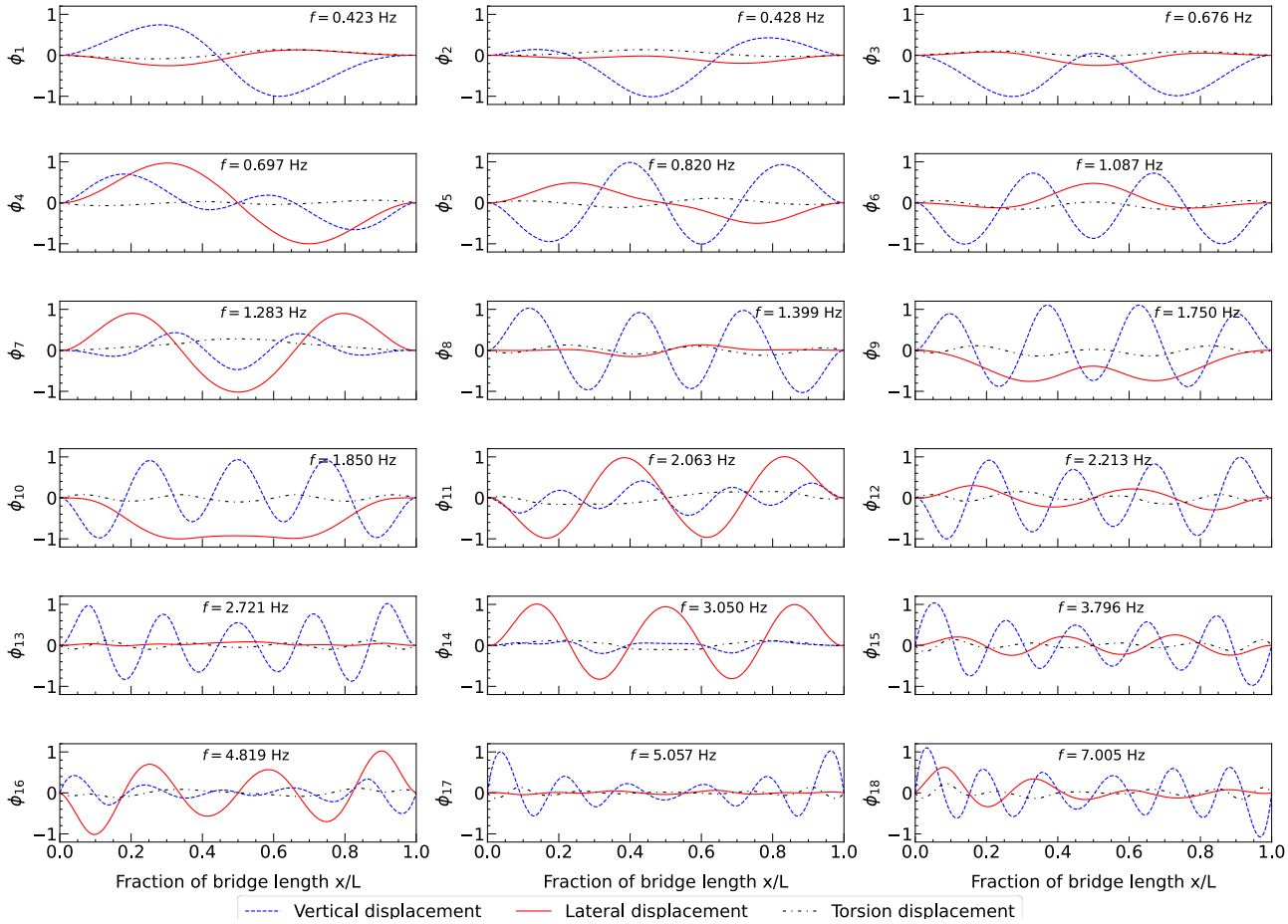

Figure 6. Mode shapes of the footbridge at wind velocity U=0 m/s right after completing the construction and before the installation of the barriers. The torsional rotation is multiplied by an amplification factor of 4 to facilitate its interpretation.

Figure 7. Figure of the section model. (a) Top view of the sectional model during its construction, (b) Bottom view of of the sectional model, (c) Sectional model inside the test chamber, and (d) sectional model tested at large angles of attack.

3 Wind tunnel tests

The aerodynamic and aeroelastic characteristics of the deck-cross sections are obtained by sectional model wind tunnel tests at the aerodynamic wind tunnel (TUVA) at the University of La Coruña [4, 5], in Spain. Sectional tests provide the time-averaged steady-state force coefficients as a function of the angle of attack. A 1:15 scale sectional model was built using a 3D printer to guarantee accurate reproduction of the deck geometry. Figure 7 shows one of the sectional models used in this study. The force coefficients used for the aerostatic stability analysis are shown in Figure 8.

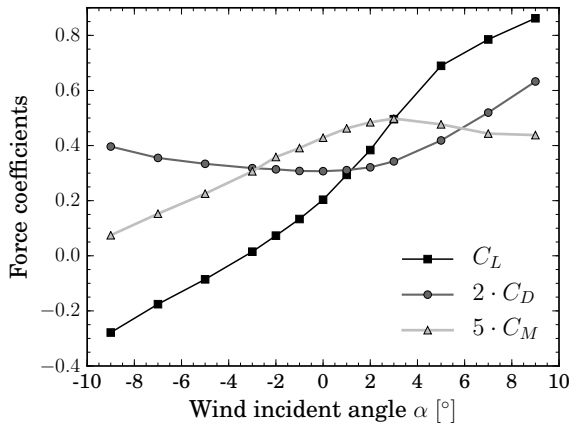

Figure 8. Force coefficients as a function of the angle of attack.

4 Static deformation: Influence of lift- and drag-induced rotation

Previous studies on the aerostatic stability of long-span bridges highlighted the importance of considering the three components of displacement-dependent wind loads in the analysis. In the case of long-span bridges with a straight deck configuration, the drag-induced rotation has a relevant impact on the rotation, which is commonly driven by the moment. Depending on the structural configuration, typically controlled by the cable supporting system, the drag-induced rotation can be positive or negative. For instance, Boonyapinyo et al. 2006 [6] reported a drag-induced nose-down rotation for the Akashi Kaikyo Bridge, which helped to delay the critical speed. Conversely, Cid Montoya et al. 2021 [1] reported a drag-induced nose-up rotation, which contributed to a decrease in the critical wind velocity, given that this effect increased the rotation generated by the moment.

The uplift effect on decks has always impacted the degradation of the bridge stiffness [7] since it helps decrease the tensions in the stays. However, the lift force commonly has no effect on the deck rotation, at least for standard bridge deck configurations. However, for curved decks, as is the case of the footbridge studied in this paper, the lift-induced rotation can impact the aerostatic stability of the bridge. Figure 9 shows the rotation of the bridge under the individual action of each of the three components. It can be seen that the effect of the drag is very low, which is reasonable due to the geometrical stiffness provided by the deck's curvature. However, the lift-induced rotation produces a rotation with a similar magnitude to the moment-induced rotation. This is possible thanks to the relationship between the bending and torsional properties of curved structures, which drastically changes the expected aerostatic behavior of this structure for both its aerostatic response and stability. The red line in Figure 9 shows the addition of the three components, which highlights the impact of the lift-induced rotation on the total deck rotation.

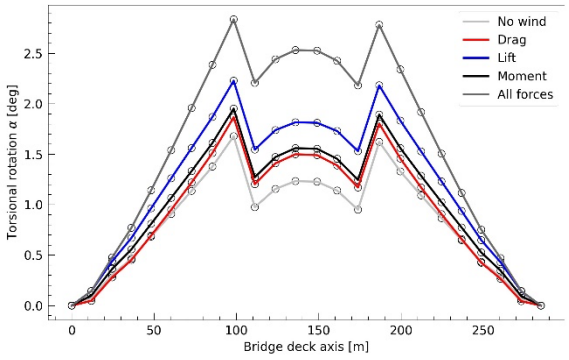

Figure 9. Comparison of the deck rotation induced by individually applied drag, lift, and moment wind load components.

5 Nonlinear aerostatic stability

5.1 Fast convergence modal-based nonlinear aerostatic stability analysis method

This method was proposed by the authors [1] seeking the acceleration of the analysis by reducing the number of iterations in the outer loop and facilitating the analysis using data easily obtained from commercial FEM software, such as the structure model shapes and natural frequencies, instead of working with the stiffness of flexibility matrices [8-10]. The basic idea is to calculate the displacements from the modal properties [11] as

$$\mathbf{u}(t) = \sum_{i=1}^{n} \mathbf{u}_i\,(t) = \sum_{i=1}^{n} \xi_i\,(t)\boldsymbol{\phi}_i = \boldsymbol{\Phi}\xi(t) \tag{1}$$

Where ξ_i stands for the modal coordinates and $\emptyset_i$ is the *i*th eigenvector. Substituting this equation into the dynamic equation of motion without damping yields:

$$\mathbf{M}\boldsymbol{\Phi}\ddot{\xi}(t) + \mathbf{K}\boldsymbol{\Phi}\xi(t) = \mathbf{f}(t) \tag{2}$$

By pre-multiplying all terms by $\boldsymbol{\Phi}^T$ we get:

$$\boldsymbol{\Phi}^T\mathbf{M}\boldsymbol{\Phi}\xi(t) + \boldsymbol{\Phi}^T\mathbf{K}\boldsymbol{\Phi}\xi(t) = \boldsymbol{\Phi}^T\mathbf{f}(t) \tag{3}$$

This is an uncoupled system because $\boldsymbol{\phi}_i{}^T\mathbf{M}\boldsymbol{\phi}_i = 1$ and $\boldsymbol{\phi}_i{}^T\mathbf{K}\boldsymbol{\phi}_i = \omega_i^2$ if the modes are orthonormal with respect to the mass. By ignoring the dynamic terms, we got the following expression without time-dependent elements:

$$\omega_i^2\xi_i = \boldsymbol{\phi}_i{}^T\mathbf{f} \tag{4}$$

Introducing eq. (4) into eq. (1), we get:

$$u_i = \frac{\boldsymbol{\phi}_i{}^T\mathbf{f}\boldsymbol{\phi}_i}{\omega_i^2}$$

Which permits the calculation of the displacements using the footbridge dynamic properties. By calculating the response at different wind velocities, led by a root-finding algorithm searching the instability point, the aerostatic critical wind velocity can be obtained. The nonlinearities of the structure are considered by updating the dynamic properties for each wind-induced deformation.

5.2 Nonlinear deformation at high wind velocities and stiffness degradation

Figures 10, 11, and 12 show the displacements along the deck for different values of wind velocities in order to show the effect of the stiffness degradation.

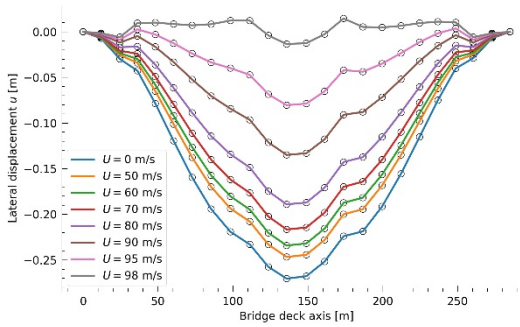

Figure 10. Lateral displacements along the deck for wind velocities U=[0,50,60,70,80,90,95,98]m/s

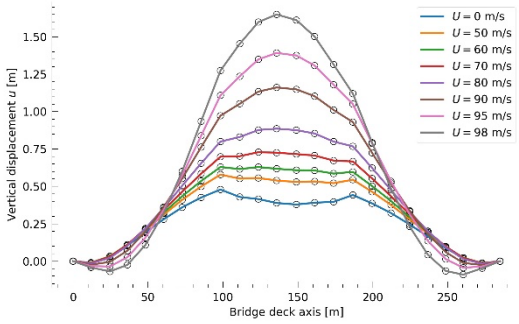

Figure 11. Vertical displacements along the deck for wind velocities U=[0,50,60,70,80,90,95,98]m/s

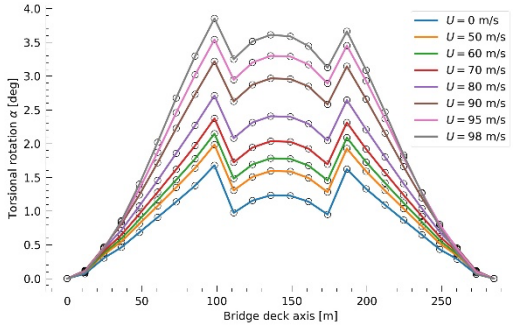

Figure 12. Torsional rotations along the deck for wind velocities U=[0,50,60,70,80,90,95,98]m/s

The uplift diminishes the stress in the cables, particularly in the main cable of the suspension system, which inevitably leads to the stiffness degradation of the footbridge. Figure 13 shows the evolution of the main natural frequencies as a function of the wind velocity. The drop in the values of the natural frequencies is particularly notable for the first two modes, which decrease their value at 98 m/s to less than half of their original value.

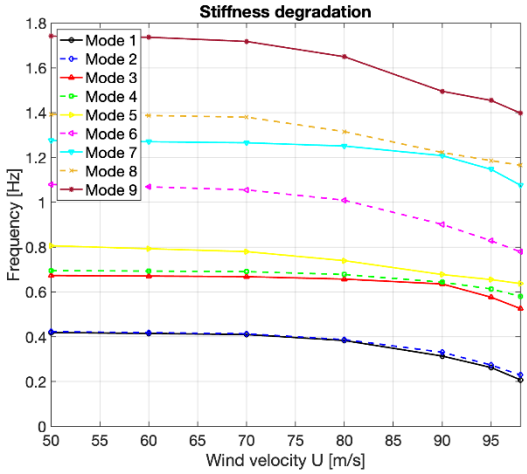

Figure 13. Variation of the natural frequency values as a function of the wind velocity due to the displacement-induced stiffness degradation

5.3 Aerostatic instability

Figure 14 shows the stiffness degradation of the structure by means of the expected linear critical velocity computed as a part of the procedure described in Section 5.1. The reader is referred to [1] for more details on the process. The value obtained for the aerostatic critical wind velocity is U_{as} = 98.2 m/s, which is higher than the flutter critical wind velocity reported by Jurado et al. 2023 [12] of U_{as} = 80 m/s. However, according to [13, 14], keeping the aerostatic critical wind velocity above the flutter critical wind velocity is always recommended, which highlights the need to conduct the aerostatic stability analysis along with flutter stability analysis. If a better performance is required, the deck cross-section can be tailored to improve the aeroelastic responses of the bridge [15, 16].

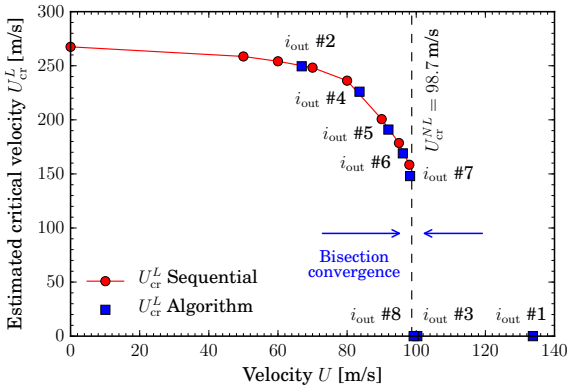

Figure 14. Convergence of the root-finding modal-based nonlinear aerostatic analysis method.

6 Conclusions

Very slender footbridges must be designed considering all potential wind-induced responses to guarantee the structure's integrity along its life cycle. Long-span footbridges can be sensitive to wind-induced phenomena, and consequently, a complete wind-resistant study must be conducted, including a complete analysis of their aerostatic stability performance. The analyses conducted in this investigation for the Gioán footbridge highlighted the importance of the lift-induced rotation on the total torsion and in the aerostatic response and stability, a feature not commonly found in other long-span structures. Hence, the three degree-of-freedom responses and the three components of the displacement-dependent wind loads must be carefully considered to reproduce the footbridge aerostatic response and stability accurately.

7 Acknowledgments

Miguel Cid Montoya is supported by the NSF under grant CMMI #2301824 and the new faculty start-up funds provided by Texas A&M University-Corpus Christi. José Ángel Jurado is supported by the Spanish Ministry for Science and Innovation in the frame of the research project PID2019-110786GB-I00.

8 References

[1] Cid Montoya, M., Hernández, S., Kareem, A., and Nieto, F., 2021 Efficient modal-based method for analyzing nonlinear aerostatic

stability of long-span bridges. Eng Struct, 244:112556.

[2] Quintela, J., Jurado, J.Á., Rapela, C., Álvarez, A. J., Roca, M., Hernández, S., Cid Montoya, M., López, J. M., Ruiz, A. J., Moreno, I. and Jiménez, S. 2020. Experimental and computational studies on the performance of solar trackers under vortex shedding, torsional divergence, and flutter. Int. J. Comp. Meth. and Exp. Meas., 8(4):387–404.

[3] Rodriguez-Segade Alonso, M., Cid Montoya, M. and Hernández, S. Wing nonlinear aerostatic stability analysis using an efficient modal-based approach. In AIAA SCITECH 2023 Forum, 0188, 2023.

[4] Jurado, J. A., Hernández, S., Nieto, F., and Mosquera, A., 2011. Bridge Aeroelasticity: Sensitivity Analysis and Optimal Design. WIT press.

[5] Jurado, J. A., Hernández, S., Cid Montoya, M., Álvarez, A. J., Nieto, F., 2016. Aeroelastic analyses of the deck widening of the Rande cable-stayed Bridge in Vigo (Spain). 8th International Colloquium on Bluff Body Aerodynamics and Applications BBAA VIII, Boston, MA, USA.

[6] Boonyapinyo V, Lauhatanon Y, Lukkunaprasit P. Nonlinear aerostatic stability analysis of suspension bridges. Eng Struct 2006;28:793–803.

[7] Zhang ZT, Ge YJ, Yang YX. Torsional stiffness degradation and aerostatic divergence of suspension bridge decks. J Fluids Struct 2013;40:269–83.

[8] Simiu, E. and Scanlan, R.H., 1996. Wind effects on structures. John Wiley and Sons, New York, NY, USA.

[9] Boonyapinyo V, Miyata T, Yamada H. Advanced aerodynamic analysis of suspension bridges by state-space approach. J Struct Eng 1999;125:1357–66.

[10] Cheng J, Jiang J-J, Xiao R-C, Xiang H-F. Nonlinear aerostatic stability analysis of Jiang Yin suspension bridge. Eng Struct 2002;24:773–81.

[11] Chopra AK. Dynamics of Structures: Theory and Applications to Earthquake Engineering. Prentice-Hall Inc; 1980.

[12] Jurado, J.A., Quintela, J., Hernández, S., Kusano, I. (2023) Flutter análisis of bridges with curvature in plan view. 16th International Conference on Wind Engineering (ICWE16), Florence, Italy.

[13] Su C, Luo X, Yun T. Aerostatic reliability analysis of long-span bridges. J Bridge Eng 2010;15:260–8.

[14] Wind-resistant design specification for highway bridges. China Communication Press, Beijing. JTG/T D60-01-2004 (in Chinese), 2004.

[15] Cid Montoya, M., Hernández, S., Nieto, F., and Kareem, A., 2020 Aero-structural design of bridges focusing on the buffeting response: Formulation, parametric studies and deck shape tailoring. J Wing Eng Ind Aerod, 204:104243.

[16] Cid Montoya M, Hernández S, Nieto F. Shape optimization of streamlined decks of cable-stayed bridges considering aeroelastic and structural constraints. J Wind Eng Ind Aerod 2018;177:429–55